Study of Heating Efficiency as a Function of Concentration, Size, and Applied Field in γ-Fe2O3 Nanoparticles

ARTICLE *in* THE JOURNAL OF PHYSICAL CHEMISTRY C · NOVEMBER 2012

Impact Factor: 4.77 · DOI: 10.1021/jp310771p

7 AUTHORS, INCLUDING:

Patricia de la Presa
Complutense University of Madrid
85 PUBLICATIONS **770** CITATIONS
SEE PROFILE

Yurena Luengo
Instituto de Ciencia de Materiales de Madrid
9 PUBLICATIONS **88** CITATIONS
SEE PROFILE

Rocio Costo
Instituto de Ciencia de Materiales de Madrid
29 PUBLICATIONS **597** CITATIONS
SEE PROFILE

Maria del Puerto Morales
Instituto de Ciencia de Materiales de Madrid
254 PUBLICATIONS **7,984** CITATIONS
SEE PROFILE

THE JOURNAL OF PHYSICAL CHEMISTRY C

Article

pubs.acs.org/JPCC

Study of Heating Efficiency as a Function of Concentration, Size, and Applied Field in γ-Fe_2O_3 Nanoparticles

P. de la Presa,*[,†,‡] Y. Luengo,[§] M. Multigner,[†] R. Costo,[§,⊥] M. P. Morales,[§] G. Rivero,[†,‡] and A. Hernando[†,‡]

[†]Instituto de Magnetismo Aplicado (UCM-ADIF-CSIC), P.O. Box 155, Las Rozas, Madrid 28230, Spain

[‡]Departamento de Física de Materiales, Universidad Complutense de Madrid, Madrid, Spain

[§]Departamento de Biomateriales y Materiales Bioinspirados, Instituto de Ciencia de Materiales de Madrid/CSIC, Sor Juana Inés de la Cruz 3, Campus de Cantoblanco, Madrid 28049, Spain

[⊥]Van't Hoff Laboratory for Physical and Colloid Chemistry, Utrecht University, Padualaan 8, 3584 CH Utrecht, Netherlands

Supporting Information

ABSTRACT: The specific absorption rate (SAR) of γ-Fe_2O_3 nanoparticles (NPs) under an alternating magnetic field has been investigated as a function of size, concentration, coating, liquid carrier, and frequency and amplitude of the applied magnetic field. The NPs have been synthesized by coprecipitation method with sizes ranging from 6 to 14 nm with low polydispersity (0.2) and high crystallinity degrees. The small NPs size (6−14 nm) and the value of the maximum applied field (<7.5 kA/m) allow the use of the linear response theory for the analysis of the experimental SARs values. Under this condition, Neel−Brown relaxation times of about 10^{-7} s are obtained from SAR field frequency dependence. The NPs have been immobilized in agar to investigate the heating mechanisms, i.e., inversion of the magnetic moments inside the monodomain volume or particle rotation. The results suggest that there is a critical size of around 12 nm for obtaining the most effective heating in viscous media. Furthermore, the surface modification by aminopropylsilane coating does not affect the heating efficiency, making these NPs good candidates for hyperthermia treatment as well as model samples for standardization of hyperthermia apparatus.

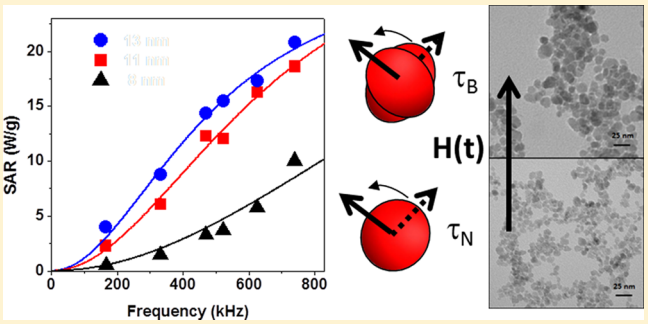

1. INTRODUCTION

The investigations on the heating efficiency of magnetic nanoparticles (MNPs) under an alternating magnetic field for tumor hyperthermia applications have increased exponentially in the last years.[1−11] The aim of most research is to find biocompatible MNPs with high specific absorption rate (SAR) values that can be synthesized in large quantities in an easy, cheap, and reproducible procedure. The present challenges are the optimization of both the exposure conditions and the MNPs characteristics and the assessment of the limits of scalability of the treatment. Unfortunately, there exists a large amount of experimental data in the literature which are not directly comparable due to SAR dependence on extrinsic parameters like field amplitude and frequency. This makes it difficult to reach a consensus about the best material or the best measurements conditions for an efficient treatment. Recently, an intrinsic loss power (ILP) parameter defined as ILP = SAR/fH_0^2 has been introduced.[12] This definition implies that the imaginary component of the magnetic susceptibility, $\chi''(t)$, is frequency-independent in the range of hyperthermia treatments (10−1000 kHz). However, there is experimental evidence that $\chi''(t)$ has a strong dependence on frequency in MNPs dispersed in a solvent, especially in the hyperthermia range.[13,14]

A theoretical frame for understanding the physical mechanism involved in MNPs heating efficiency is the linear response theory (LRT). This theory models the relaxation mechanisms if the maximum applied field amplitude H_0 satisfies $\mu_0 M_s V H_0 < k_B T$, where M_s is the magnetic saturation, V the MNPs volume, and T the absolute temperature. This condition implies that the sample magnetization depends linearly on the applied field and the maximum field amplitude is limited by particle size and saturation. In this model, the SAR depends on Brown−Neel relaxation time τ_R, field amplitude H_0, and frequency f as follows: SAR $\propto M_s^2 V H_0^2 T^{-1}[\tau_R(2\pi f)^2/(1 + (2\pi f\tau_R)^2)]$.

In the present work, we perform a systematics study of the influence of concentration, size, coating, liquid carrier, and field amplitude and frequency on SARs values of γ-Fe_2O_3 MNPs synthesized by the coprecipitation method modified to reduce the MNP size distribution.[15] The heating efficiency is expected

Received: August 16, 2012
Published: November 8, 2012

to be influenced by any parameter affecting the magnetic interactions between particles and therefore the magnetic moment rotation. In fact, magnetic interactions have been observed to significantly diminish the dipolar magnetic field outside a capsule when particles are highly packed.[16] In the same sense, SAR has been observed to increase with MNPs size up to a certain value,[17] but the dependence of this parameter on the media viscosity is not so clear.[5,13,14,18] Other important issue limiting the application of the magnetic hyperthermia is the characteristics of the magnetic field required to produce the heating, which should be within the range approved for human use to avoid overcoming the discomfort factor limit $H_0 f < 5 \times 10^9$ A·m^{-1}·s^{-1}.[11,19−21] Frequency and magnetic field amplitude strongly affect the heating efficiency of the MNPs following different trends depending on the structural, colloidal, and magnetic properties of the material that makes difficult the understanding of the phenomenon behind.

2. EXPERIMENTAL METHODS

2.1. Synthesis. Maghemite NPs were obtained following the Massart coprecipitation protocol.[22] Some modifications were introduced to control particle size between 6, 8, 11, 13, and 14 nm and to reduce size distribution below polydispersity degrees of 0.2 (standard deviation/mean size).[15]

2.1.1. Synthesis of Magnetic Nanoparticles. Magnetite (Fe_3O_4) nanoparticles were synthesized by coprecipitation of 425 mL of a mixture of $FeCl_3 \cdot 6H_2O$ (0.09 mol) and $FeCl_2 \cdot 4H_2O$ (0.054 mol) in 75 mL of alkaline medium. The particles size can be tuned by the nature of the basis used in the coprecipitation, the addition rate, and the aging time.[23] Thus, for the synthesis of the smallest particles fast addition rates (40 mL/s) and KOH (25%) and NH_4OH (25%) as alkaline solutions were used to produce the 6 and 8 nm particles, respectively. Slow addition rates (0.2 mL/s) and NH_4OH solutions were used to synthesize all the other samples (11, 13, and 14 nm). The largest particles, 13 and 14 nm, were obtained by subjecting the 11 nm particles to a heating process at 90 °C for 1 and 3 h, respectively. After every synthesis the particles were washed three times with distilled water and the help of a permanent magnet.

2.1.2. Acid Treatment. A standard protocol was used to oxidize magnetite to maghemite (γ-Fe_2O_3), which is more stable in time and suitable for biomedical applications.[15] In addition, this treatment activates the particle surface for further coating with APS. Briefly, 300 mL of HNO_3 (2 M) was added to the particles, and the mixture was stirred for 15 min. Then, nitric acid was removed by magnetic decantation, and 75 mL of $Fe(NO_3)_3$ (1 M) and 130 mL of water were added to the particles. The mixture was heated up to boiling temperature and stirred for 30 min.[15,24] The particles were then cooled to room temperature, and by magnetic decantation, the supernatant was substituted by 300 mL of HNO_3 (2 M) and stirred for 15 min. Finally the particles were washed three times with acetone and redispersed in water. A rotary evaporator was used to remove any acetone waste and concentrate the sample.

2.1.3. APS Coating. Surface modification was performed by adding very slowly (10 μL/s) 1.22 mL (0.005 mol) of (3-aminopropyl)triethoxysilane (APS) to a mixture of 10 mL of particles (28 g Fe_2O_3/L) and 10 mL of methanol, keeping strong stirring for 12 h.[25] After that, methanol was eliminated in the rotary evaporator, and rest of the APS was eliminated by dialysis.

2.2. Structural and Colloidal Characterization. The crystal structure of the samples was identified by X-ray powder diffraction (XRD) performed in a Bruker D8 Advance powder diffractometer using Cu Kα radiation. The patterns were collected between 10° and 70° in 2θ. The XRD spectra were indexed to an inverse spinel structure. The average crystallite size was calculated with the half-width of the (311) X-ray diffraction peak by means of the diffraction computer program (APD) utilities from Phillips. The error in the crystallite sizes obtained by use of the Scherrer's equation is ±0.1 nm, which is related to the instrumental line width. ($\Delta 2\theta = 0.11°$).

Particle size and shape were determined by transmission electron microscopy (TEM) and high-resolution electron microscopy (HRTEM). TEM samples were prepared by placing one drop of an aqueous dilute suspension of MNPs on a copper grid covered with a perforated carbon film and allowing the solvent to evaporate slowly at room temperature. The mean particle size and distribution were evaluated by measuring the largest internal dimension of at least 100 particles. Afterward, data were fitted to a log-normal or Gaussian distribution to obtain the mean size and standard deviation (σ) that were considered to be representative of the absolute error of the measurement.

Fourier transform infrared spectra (FTIR) were recorded between 3600 and 400 cm^{-1} in a Bruker IFS 66 V-S spectrometer. Samples were prepared by dilution of iron oxide powder in KBr at 2% by weight and compressing the mixture, pressing it into a pellet. Simultaneous thermogravimetric (TG) analysis and differential thermal analysis (DTA) were performed on a Seiko TG/DTA 320U thermobalance. Samples were heated from room temperature to 900 °C at 10 °C/min under an air flow of 100 mL/min. Colloidal properties of the samples were studied in a Zetasizer Nano S, from Malvern Instruments. The hydrodynamic size of the particles in suspensions was measured by dynamic light scattering (DLS), and the zeta potential was measured as a function of pH at 25 °C, using 10^{-2} M KNO_3 as background electrolyte and HNO_3 and KOH to change the pH of the suspensions.

The Fe concentration was measured with an inductively coupled plasma optical emission spectrometer (ICP-OES) Perkin-Elmer Optima 2100 DV. For this purpose samples were digested with nitric acid to oxidize the organic coating and then with hydrochloric acid to dissolve the particles.

2.3. Magnetic Characterization. The magnetic characterization was performed in a Quantum Design MPMS-5S SQUID magnetometer. The magnetic characterization of 75 μL iron oxide suspension at 70 $mg_{Fe_2O_3}$/mL was carried out in special closed sample holders. The characterization consists of hysteresis loops at 50 kOe and at 10 and 250 K and zero-field-cooled and field-cooled (ZFC-FC) curves from 10 to 250 K and 50 Oe applied field. The maximum temperature was 250 K in order to maintain the colloidal freeze during the magnetic characterization. Due to the large iron oxide content, the diamagnetic contribution from water at high fields can be discarded. In the case of ZFC-FC curves, the blocking temperature T_B was determined from the maximum of the ZFC curve.

2.4. Heating Efficiency. Heating capacities of MNPs have been measured with the commercial system Magnetherm 1.5 (Nanotherics). The system is provided with 2 coils of different turns and length and 5 different capacitors arrays that constitute 10 circuits with different resonant frequency, which allows

dx.doi.org/10.1021/jp310771p | J. Phys. Chem. C 2012, 116, 25602−25610

studying the effect of magnetic field frequency on the heating response of the NPs. The resonance frequency of the equipment has been tuned for each measurement. Mean magnetic field inside the coil has been measured with a secondary two turns coil with a cross-sectional value close to that of the sample holder (6.2 mm diameter). A half-length of the sample was made to coincide with the maximum value of the magnetic field. The volume sample was 1 mL. The temperatures of the coils have been controlled through a close circuit of water maintained at 16 °C with a cryostat bath. In these conditions, a water sample has been measured under the experimental conditions, and it has been checked that water temperature does not increase in the sample space.

The temperature of MNPs suspension has been measured with a fiberoptical thermometer and registered with a computer. The temperature sample has been controlled and stabilized to room temperature before each measurement. Prior to turning the magnetic field on, the sample temperature was recorded for about 60 s in order to ensure thermal stability and to have a baseline for the calculation of the SARs values. The temperature increase of the samples was measured either up to 80 °C or during 300 s.

Since the Fe concentrations are in the range 1−5 wt %, the SARs values for the magnetic hyperthermia experiments can be calculated as SAR = $(C_{water}/c_{Fe})(\Delta T/\Delta t)$, where C_{water} is the specific heat capacity of water and c_{Fe} the Fe weight concentration in the colloid.[26] By performing a linear fit of data (temperature versus time) in the initial time interval, the slope $\Delta T/\Delta t$ can be obtained. The measurements were performed in nonadiabatic conditions; thus, the curves slopes $\Delta T/\Delta t$ were fitted only in the first few seconds after the magnetic field was turned on, and the range was selected such as the slope was a maximum (1 to ∼30 s).[27] Then, the SARs values were obtained by fitting the experimental heating curves which were normalized to the iron mass (W/g_{Fe}).

The 8, 11, and 13 nm MNPs have been measured as a function of iron concentration (c_{Fe}) at H = 7.5 kA/m and f = 522 kHz. The initial concentration was the highest, and the measurements were performed by diluting the concentration in half in consecutive steps with milli-Q water and sonicating.

The effect of size on the SARs has been also investigated. Particles with diameter d = 6, 8, 11, 13, and 14 nm have been measured at H_0 = 7.5 kA/m and f = 522.7 kHz. Since the SARs values are independent of NPs concentration (as will be discussed later), the concentration 50 mg/mL has been chosen for this part of the experiment because it is high enough to obtain heating curves that can be properly fitted and low enough to discard the MNPs specific heat capacities in the colloid.

The magnetic colloid has been also characterized as a function of field amplitude for particles dispersed in water or immobilized in agar in order to investigate the mechanism involved in the heating process. For this purpose, 50 mg/mL of the colloidal suspension in water or agar at 1 wt % was measured at 522.7 kHz with the field amplitude varying from 2.4 to 7.5 kA/m for the 13 and 14 nm particle sizes and from 4 to 7.5 kA/m for the rest. The temperature of the agar suspension was not allowed to exceed 50 °C to avoid the melting of agar. Due to temperature increase in the colloid depends on MNPs concentration, a concentration of 100 mg/mL of the 13 nm MNPs aqueous colloid was used to get experimental data at very low fields (lower than 2.4 kA/m). The measurements were performed at 522.7 kHz with the field amplitude ranging from 0.8 to 7.5 kA/m with a 0.4 kA/m step.

The SAR field frequency dependence was measured at H_0 = 4 kA/m amplitude field for the 8, 11, and 13 MNPs sizes at frequencies 166.0, 330.9, 468.8, 522.8, 626.7, and 739.2 kHz, and the concentration was c_{Fe} = 50 mg/mL.

APS-coated MNPs were measured at H_0 = 7.5 kA/m and f = 522.3 kHz. The concentrations was c_{Fe} = 8 mg/mL for the 8 and 13 nm MNPs sizes.

All the SAR values were obtained under experimental condition $H_0 f < 5 \times 10^9$ $A/m^{-1}\,s^{-1}$, a limit at which an unwanted nonselective heating of both cancerous as well as healthy tissue due to generation of body eddy currents may occur.[21]

3. THEORETICAL MODEL

3.1. The Linear Response Theory (LRT) Model. This theory aims to calculate the hysteresis loop area and shape when the magnetic response is linear with the applied magnetic field, which is satisfied under the condition $\mu_0 M_s V H_0 < k_B T$, where μ_0 is the vacuum permeability, M_s the saturation magnetization, V the particle volume, H_0 the field amplitude, k_B the Boltzmann constant, and T the absolute temperature.[28]

The magnetic moment of a particle suspended in a fluid can relax after magnetic field removal by two different mechanisms: the Neel and Brown relaxations.[9,13,14] The relaxation times can be then described by Neel relaxation time τ_N

$$\tau_R = \tau_N = \tau_0 e^{K_{eff} V/k_B T} \tag{1}$$

or by Brown relaxation time τ_B

$$\tau_R = \tau_B = \frac{4\pi\eta r_h^3}{k_B T} = \frac{3\eta V_h}{k_B T} \tag{2}$$

where η is the viscosity of the fluid and r_h the hydrodynamic radius of the particle.

In a general case, both mechanisms are present, but the faster relaxation mechanism is dominant and an effective relaxation time may be defined by

$$\frac{1}{\tau_R} = \frac{1}{\tau_B} + \frac{1}{\tau_N} \tag{3}$$

The crossover between Neel and Brown relaxation regimes depends, for a given size, on effective anisotropy and media viscosity. The Neel relaxation time depends exponentially on volume whereas the Brownian relaxation varies linearly with it.

Finally, within the validity of LRT, the loss power density P for randomly oriented magnetic NPs is given by[28]

$$\begin{aligned} P &= 2\mu_0 \pi \chi''(t) f H_0^2 \\ &= \frac{\mu_0 \chi_0 H_0^2}{\tau_R} \frac{(2\pi f \tau_R)^2}{1 + (2\pi f \tau_R)^2} \\ &= \frac{\mu_0^2 M_s^2 V H_0^2}{3 k_B T \tau_R} \frac{(2\pi f \tau_R)^2}{1 + (2\pi f \tau_R)^2} \end{aligned} \tag{4}$$

The loss power density P ($W\,m^{-3}$) is related to the specific absorption rate SAR ($W\,g^{-1}$) by the mean mass density of the particles (SAR = $P/\rho_{Fe_2O_3}$).

Therefore, in the LRT the SARs depend on several parameters: it increases linearly with the NPs volume and quadratically with the field amplitude. Furthermore, the

dx.doi.org/10.1021/jp310771p | J. Phys. Chem. C 2012, 116, 25602−25610

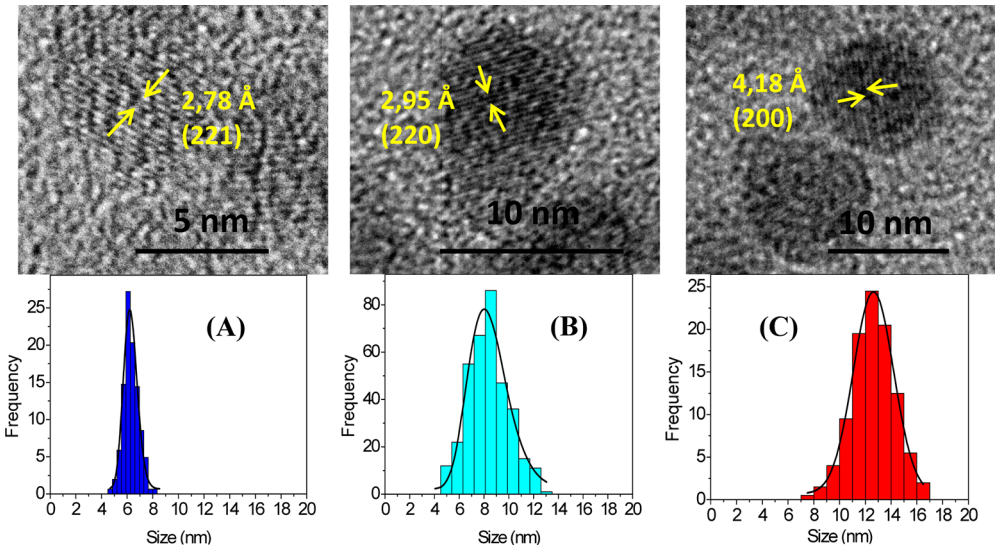

Figure 1. HRTEM micrographs and size distribution of (A) 6, (B) 8, and (C) 13 nm MNPs.

Table 1. Experimental Results on Mean Particle Sizes Measured by TEM, Hydrodynamic Sizes at pH 3 and pH 7, and Isoelectric Points of Charges (IEP) before and after APS Particle Coating Characterized by DLS[a]

sample	mean particle size by TEM (nm)	hydrodynamic size at pH 3 (nm)	hydrodynamic size at pH 7 (nm)	IEP (before coating)	IEP (after coating)
6	6.3 (0.2)	48 (0.2)	49 (0.2)	8.3	10.2
8	8.3 (0.2)	37 (0.2)	55 (0.2)	7.6	10.1
11	10.6 (0.2)	48 (0.2)	62 (0.2)	7.9	9.5
13	12.7 (0.2)	60 (0.2)	75 (0.2)	6.5	9.2
14	13.7 (0.2)	106 (0.2)	68 (0.2)	8.0	10.0

[a]Polydispersity degree (standard deviation/mean size) is included between brackets.

frequency dependence has three different regimens: (i) for low frequencies such as $2\pi f\tau_R < 1$, the loss power increases quadratically with the frequency, (ii) at very high frequencies $2\pi f\tau_R \gg 1$, the loss power saturates to the value $P = (\mu_0\chi_0 H_0^2)/\tau_R$, and (iii) for intermediate values of the frequency, the loss power varies with the expression given in eq 4.

Due to SAR dependence on parameters which are extrinsic to the NPs properties, as ac field amplitude and frequency, the comparison of reported SAR values does not give much information on the NPs heating efficiency. More recently, an intrinsic loss power parameter defined as ILP = SAR/(fH_0^2) has been proposed in order to compare heating efficiencies obtained under different experimental conditions.[12] The definition of ILP parameter regards the magnetization losses as frequency-independent, allowing direct comparison of the particle-heating capabilities independently of the applied ac field strengths and frequencies. However, this approximation is not always satisfied by particles in suspensions; a nonlineal behavior of susceptibility imaginary part in MNPs is reported by different authors.[13,29] Moreover, our results show also a nonlineal frequency dependence of the SARs.

4. RESULTS AND DISCUSSION

4.1. Structural, Colloidal, and Magnetic Properties.

Maghemite NPs with increasing diameters from 6 up to 14 nm have been synthesized by coprecipitation by controlling different experimental parameters. Particle size obtained by TEM (Figure 1, Table 1, and Figure S1 of the Supporting Information) is confirmed by XRD diffractograms (Figure S2 (Supporting Information)); the diffraction peaks become broader as the NPs sizes decrease. Particle size distribution was reduced from 30% to 20% by an acid treatment of the particles that has been previously shown to dissolve the smallest particles and recrystallize the largest ones mainly at the surface, leading to highly crystalline particles with improved magnetic properties.[15] Suspensions at high Fe concentration (over 200 mg Fe/mL) were obtained following an easy and reproducible synthesis method and keeping under control experimental parameters such as reagent concentration, addition rate, temperature, and reaction time.

The MNPs form highly concentrated (over 200 mg Fe/mL) stable colloidal suspensions at acidic or basic pH values (Figure 2). The isoelectric point of charge (IEP) is around 7, which is

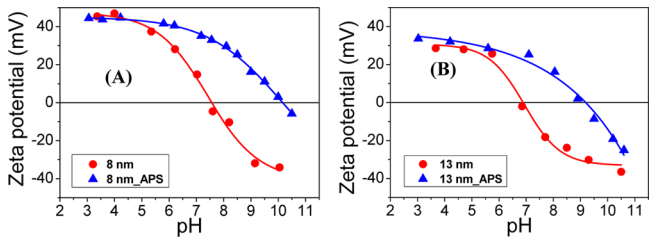

Figure 2. Zeta potential of (A) 8 nm and (B) 13 nm uncoated (full circles) and APS-coated (full triangles) γ-Fe_2O_3 MNPs.

in good agreement with previous values reported for IEP of maghemite.[30,31] Hydrodynamic sizes at acidic pH are below 50 nm for the smallest particles (6, 8, and 11 nm) and around 70–80 nm for the largest ones. Since the IEP is close to 7, the dispersions are not stable at physiological pH and need to be further coated to make a material suitable for biomedical

dx.doi.org/10.1021/jp310771p | J. Phys. Chem. C 2012, 116, 25602–25610

applications. Table 1 summarizes the experimental results on particle size as well as the hydrodynamic sizes and IEPs for the uncoated and APS-coated MNPs.

Aminopropylsilane coating has been proposed as an excellent material to stabilize MNPs at pH 7 and to provide positive charged groups at the NP surface (see Figure 2) that can be used to attach other biomolecules.[32] In light of the FTIR and thermogravimetric results, APS was covalently bonded to the particle surface (see Supporting Information, Figures S3–S6). Hydrodynamic size was only slightly altered by the coating while IEP was shifted to higher pH values (>9) leading to suspensions with a wider pH range of colloidal stability (Table 1, Figure 2, and Figure S7). At physiological pH, the z-potential of the coated samples is over 30 mV providing long-term stability of the dispersions.

Hysteresis loops at 250 K for all samples in the form of aqueous suspensions showed nearly superparamagnetic behavior with negligible coercivity (<10 Oe) and remanent magnetization (Figure 3A). At 10 K and 50 kOe, the magnetic

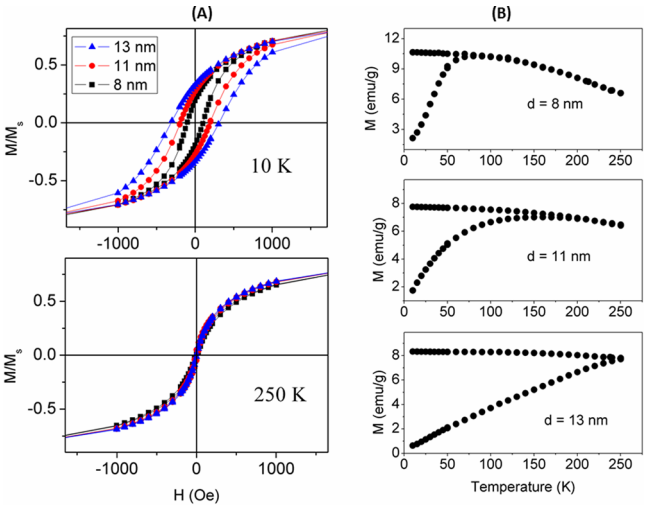

Figure 3. Hysteresis cycles and ZFC-FC curves for 8, 11, and 13 nm sizes: (A) Normalized hysteresis curves at 10 and 250 K; (B) ZFC-FC at 50 Oe applied field.

saturation is 68–70 emu/g for MNPs sizes larger than 8 nm, close to the bulk value. At low temperature, the coercivity increases with size: 100, 200, and 300 Oe for the 8, 11, 13 NPs sizes, respectively (see Figure 3A). Due to the small NPs sizes, the magnetic behavior is in the monodomain regime; therefore, the coercive field depends on effective magnetic anisotropy K_{eff}, saturation magnetization M_s, particle volume V, and absolute temperature T as follows:[33]

$$H_c = \left(\frac{2K_{eff}}{\mu_0 M_s}\right)\left(1 - \left(\frac{25k_BT}{K_{eff}V}\right)\right)$$

If M_s and K_{eff} are volume-independent, then the coercive field decreases as size decreases as observed for these samples. However, it has been reported that for small MNPs the coercivity increases as size decreases due to surface anisotropy contribution that increases K_{eff} to values much larger than that expected for the bulk magnetocrystalline anisotropy.[23,34,35] As in our samples M_s is almost the same for the three sizes, then the size dependence of the coercivity observed here (decrease of the coercivity with decreasing size) reflects the high degree of crystallinity of these particles, assuming that K_{eff} is nearly volume-independent.

The ZFC-FC curves show an increase in blocking temperature (T_B) as size increases. T_B varies from 70 to 130 K for the 8 and 11 nm NPs, whereas for the 13 nm it is around 250 K. The behavior is related to the increase of the magnetocrystalline energy due to the increasing particle volume (see Figure 3B) and agrees well with reported data.[36,37]

4.2. Specific Absorption Rate (SAR). *4.2.1. SAR as a Function of Concentration and Size.* Figure 4 shows the experimental hyperthermia curves for different (A) concentrations, (B) sizes, and (C) carrier liquids. The results of SARs measured as a function of concentration for the 8, 11, and 13 nm NPs are shown in Figure 5A. The NPs synthesized in this work can be concentrated up to 300 mg/mL at acidic pH with colloidal stability that can last for months. For each NP size, SAR is almost constant in the iron concentration range investigated here from ~6 to ~300 mg/mL. Other works on iron oxide NPs have shown a SAR decrease when Fe concentration decreases below 5 mg/mL.[38]

As can be seen from Figure 5A, there is a significant increase of a factor 4 in the SAR values for the 8 to the 11 nm size from ~10 to ~40 W/g, respectively, whereas for the 11 and 13 nm, the SAR increases only by a factor ~0.4 (from ~40 to ~55 W/g). In Figure 5B, the SAR has a near cubic dependence on the NP radius, as expected from the LRT when M_s, H_0, and f are constant.

The samples are synthesized at high concentrations (200–300 mg/mL) and then diluted by adding Milli-Q water and

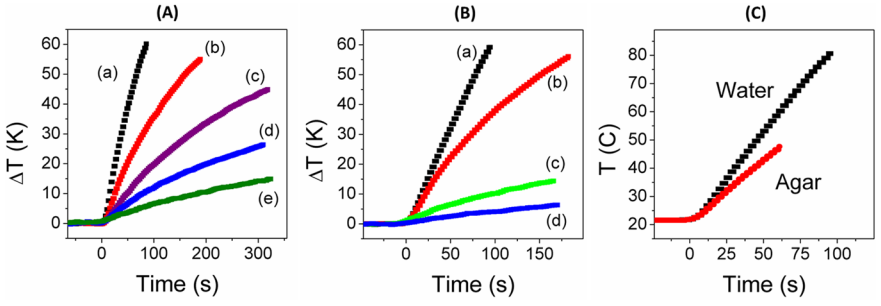

Figure 4. (A) Temperature increases of the magnetic colloidal suspension for the 11 nm MNPs as a function of concentration: (a) 100, (b) 50, (c) 25, (d) 12.5, and (e) 6.25 mg/mL. (B) Experimental heating curves for different sizes: (a) 13, (b) 11, (c) 8, and (d) 6 nm. For the sake of clarity, since the experimental values corresponding to d = 14 nm are close to that of d = 13 nm, they have been excluded from the graph. The measurements were performed at c_{Fe} = 50 mg/mL. (C) Temperature dependence of 14 nm MNPs dispersed in water and in agar at c_{Fe} = 50 mg/mL. All the experimental heating curves were performed at applied magnetic field H_0 = 7.5 kA/m and f = 522.7 kHz.

dx.doi.org/10.1021/jp310771p | J. Phys. Chem. C 2012, 116, 25602–25610

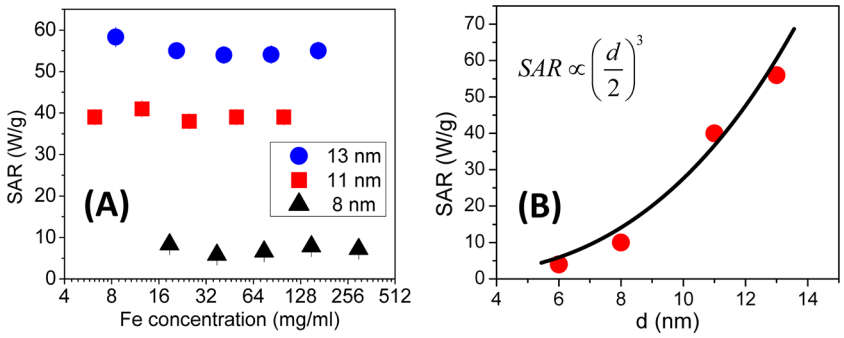

Figure 5. (A) SAR vs Fe concentration for 8, 11, and 13 nm MNPs. (B) SARs values as a function of nanoparticles size. The measurements have been performed at H_0 = 7.5 kA/m and f = 522.7 kHz.

sonicating. MNPs form aggregates in order to diminish the magnetostatic energy. The effective field acting on a particle is the sum of the applied field and the field produced by the surrounding particles in the cluster. The cluster sizes (number of MNPs inside the aggregates) can be inferred from the hydrodynamic size and are then determined by particle size and initial concentration (high MNP concentration) as shown in Table 1. The subsequent dilution and sonication cannot separate the particles inside the aggregates but instead separate the aggregates. Therefore, the magnetic interaction between MNPs inside the clusters should remain almost constant because interparticle distance is not affected by dilution whereas the magnetic interactions between aggregates could change with dilution. The fact that SAR does not vary with MNPs concentration suggests either that interaction between clusters does not appreciably change for this concentration range or that its influence on the heating efficiency could be disregarded.

4.2.2. SARs as a Function of Field Amplitude and Frequency. Using the LRT model and SAR experimental values, relaxation times and effective anisotropy can be evaluated under $\mu_0 M_s V H_0 < k_B T$ conditions. In Figure 6, the

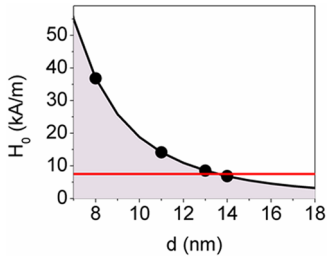

Figure 6. Gray area under the curve representing the magnetic field amplitudes that satisfy the condition $\mu_0 M_s V H_0 < k_B T$ of the LRT at room temperature for different particle sizes (the full black line represents $\mu_0 M_s V H_0 = k_B T$). The maximum applied field in this work was 7.5 kA/m (red line).

gray area under the curve represents the maximum field amplitudes as NPs size function that allow the analysis of the results in the framework of the LRT. The maximum applied field in this work was 7.5 kA/m, which is well below the maximum for all NPs, except for the 14 nm size that was 4 kA/m.

The frequency dependence of the SARs has been fitted with a function of the form

$$h(f) = a\frac{\tau_R(2\pi f)^2}{1 + (2\pi f\tau_R)^2} \quad (5)$$

that fits eq 4 with $a = (\mu_0^2 M_s^2 V H_0^2)/(3k_B T\rho_{Fe})$. Figure 7 shows the theoretical curve (A) and the experimental results and fits

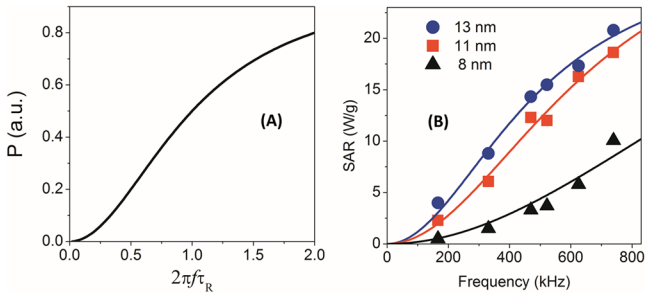

Figure 7. (A) Representation of the loss power density (P) (eq 4) with arbitrary units as a function of $2\pi f\tau_R$ in the range [0, 2]. (B) Experimental SARs frequency dependence for d = 8, 11, and 13 nm MNPs (triangles, circles, and squares). The full lines represent the fits with eq 4. The measurements have been performed at H_0 = 4 kA/m and c_{Fe} = 50 mg/mL.

Table 2. Fitted Parameters a (J/g) and τ_R (s) Obtained by Fitting SAR Frequency Dependence with Eq 5[a]

	a (J/g)	τ_R (s)	τ_B (s)	K_{eff} (J/m^3)
13 nm	9.5(1) 10^{-6}	3.3(3) 10^{-7}	8.3 × 10^{-7}	2.1(2) 10^4
11 nm	8.1(1) 10^{-6}	2.4(2) 10^{-7}	5.0 × 10^{-7}	3.3(3) 10^4
8 nm	3.0(30) 10^{-6}	0.9(10) 10^{-7}	1.9 × 10^{-7}	6.7(10) 10^4

[a]Brownian relaxation times τ_B are calculated with eq 2. Effective anisotropy K_{eff} is estimated considering $\tau_R = \tau_N$ and $\tau_0 = 10^{-9}$ s in eq 1.

(B) and Table 2 the fitted values. The advantage of the fitting is that it is possible to obtain the relaxations times directly from the fit. The parameter a varies with the NPs volume if M_s, H_0, and T are the same for the three samples, as is the case. If we neglect the size distribution, then the relationship V_1:V_2:V_3 is 1:1.65:4.3. However, the obtained relation between a's parameters a_1:a_2:a_3 is 1:1.25:3 and deviates slightly from that of the volume as expected since the effect of NPs size distribution has not been taken into account. As a first approximation, a fits the volume variation.

As can be observed from Figure 7B, the SARs dependence for the smaller NPs behaves nearly quadratically with frequency; therefore, the fitting of the parameters a and τ_R

dx.doi.org/10.1021/jp310771p | J. Phys. Chem. C 2012, 116, 25602−25610

with eq 5 produces large uncertainties. The fitted value of τ_R indicates that the 8 nm NPs are in the regime $2\pi f\tau_R < 1$ even for the largest frequency used in this work f = 739.2 kHz. However, the trend of the a parameter looks quite similar to that observed for the larger NPs.

The fitted relaxation times τ_R obtained are about 10^{-7} s, which agree well with relaxation times for γ-Fe_2O_3 in the frequency range investigated here.[5] The Brownian relaxation time τ_B was calculated with eq 2 for MNPs dispersed in water considering the water viscosity η = 1 cP and the hydrodynamic radius r_h as the particle radius (because of the lack of particle surfactants). For MNPs dispersed in water, Table 2 compares τ_B with the fitted τ_R. Although $\tau_R < \tau_B$, both relaxation times are of the same order of magnitude. If the MNPs are suspended in a more viscous media like agar, then the Brownian relaxation times τ_B increase (see eq 2). Figure 4C shows the different temperature dependence of NPs dispersed in water and in agar.

The effective anisotropy, K_{eff}, can be estimated considering the fitted τ_R as a good approximation of the Neel relaxation time: $\tau_R = \tau_0 e^{(K_{eff}V)/(k_BT)}$, with $\tau_0 \approx 10^{-9}$ s (see Table 2). Besides, K_{eff} can be independently estimated from ZFC-FC curves by considering that blocking temperature T_B, particle volume V, and K_{eff} satisfy the relation $K_{eff}V \approx 25k_BT_B$. ZFC-FC curves in Figure 3B show a broad T_B distribution for the 11 and 13 nm MNPs that makes difficult the determination of T_B. However, the 8 nm MNPs show a T_B around 70 K giving an estimated K_{eff} around 9×10^4 J/m^3, close to the value found by calculating K_{eff} by means of the relaxation time τ_R in eq 1, i.e., 6.7×10^4 J/m^3 (see Table 2). The similarity between both anisotropy values reinforces our hypothesis that the main mechanism contributing to the magnetization rotation for particles 8 nm in diameter is Neel relaxation. However, these anisotropy values are large compared to the bulk anisotropy at room temperature $K_1 = 4.64 \times 10^3$ J/m^3 of γ-Fe_2O_3[39] which means that surface or shape anisotropy effects cannot be discarded.

The field amplitude dependence of experimental SARs has a near quadratic behavior as expected by the LRT. A thorough characterization of SAR as a function of field amplitude from 0.8 to 7.5 kA/m with a 0.4 kA/m step is shown in Figure 8 for the 13 nm NPs at c_{Fe} = 100 mg/mL and f = 522.7 kHz. A data fit performed with a function of the form $SAR(H_0) = cfH_0^2$ gives

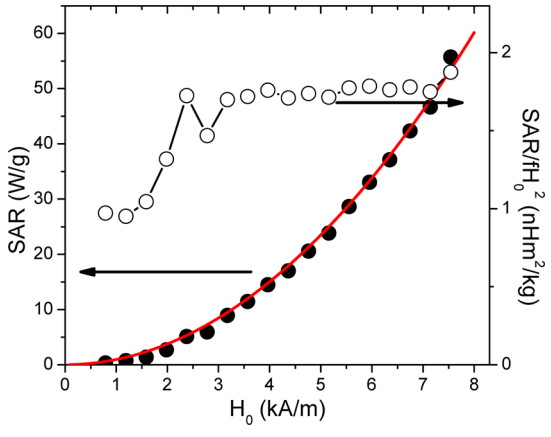

Figure 8. Field amplitude dependence of SAR for the 13 nm NPs at c_{Fe} = 100 mg/mL and f = 522.7 kHz (full circles, left scale); the red line represents a fit of the form SAR = cfH_0^2. The open circles (right scale) represent the values of SAR/cfH_0^2.

c = 1.78(1) nH m^2/kg with a determination coefficient R^2 = 0.997. The R^2 value close to 1 means high fit accuracy. The parameter c is directly the ILP which has been defined as ILP = SAR/fH_0^2.[12] However, if the ILP is calculated for each field amplitude (see Figure 8, right scale), it matches fitted c parameter only for field amplitudes higher than 2.4 kA/m, which then looks like a threshold field to induce the material response.

4.2.3. SAR as a Function of Matrix and Coating. The MNPs were measured in different liquid carriers (water and agar) in order to elucidate the heating mechanism that takes place at different particle sizes. As can be seen from Figure 9

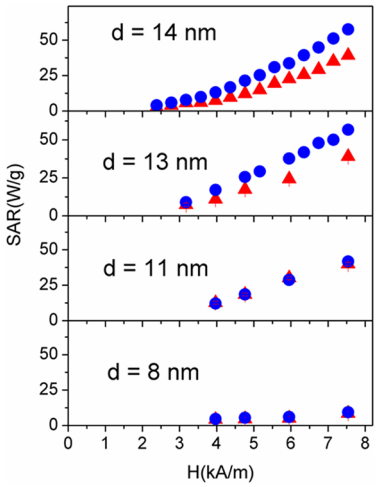

Figure 9. Field amplitude dependence of the SARs values for d = 8, 11, 13, and 14 nm MNPs dispersed in water (full circles) and in agar (full triangles). For the 8 and 11 nm MNPs, the SARs values in water and agar overlap. The measurements have been performed at c_{Fe} = 50 mg/mL and f = 522.3 kHz.

Table 3. SARs Values for Uncoated and APS-Coated γ-Fe_2O_3 MNPs Dispersed in Water or Agar[a]

	SAR (W/g$_{Fe}$)		
	uncoated MNPs (50 mg$_{Fe}$/mL)		APS-coated MNPs (8 mg$_{Fe}$/mL)
size (nm)	water	agar 1 wt %	water
6	4(1)	–	–
8	10(1)	10(1)	8(1)
11	42(1)	40(1)	–
13	55(1)	41(1)	56(1)
14	58(1)	40(1)	–

[a]The values were obtained at H_0 = 7.5 kA/m and f = 522.3 kHz. The product $H_0f = 4 \times 10^9$ A/m^{-1}s^{-1} does not overcome the safe limit for application of hyperthermia to patient.

and Table 3, the SAR values fall for the larger MNPs when they are dispersed in agar, whereas for the smaller ones the heating efficiency seems to be independent of the media viscosity. Although the agar viscosity depends on average molecular weight, concentration, and type, its viscosity η can be more than 20 times larger than water viscosity,[40] high enough to considerer the MNPs are nearly immobilized.

The similar SAR values obtained for the smallest MNPs dispersed in water and in agar evidence that the heating

dx.doi.org/10.1021/jp310771p | J. Phys. Chem. C 2012, 116, 25602−25610

efficiency is not significantly affected by the media viscosity (see Figure 9). If we assume that the MNPs are quasi-immobilized in agar, the heat production mechanism is the inversion of the magnetic moments inside the monodomain volume. On the other hand, the heating efficiency clearly diminishes when the larger MNPs are dispersed in agar suggesting that a different mechanism is responsible for the heat production. It is observed from Table 3 that the maxima SARs for the larger MNPs (13 and 14 nm) dispersed in agar are close to the maximum SAR value for the 11 nm MNPs.

Actually, the relaxation times calculated here do not take into account the NP size distribution. A simple calculation of the relaxation times as a function of size by means of eqs 1 and 2 shows smaller MNPs would relax by a Neel relaxation process whereas the Brown relaxation mechanism controls the relaxation process for the larger sizes (Figure 10). However,

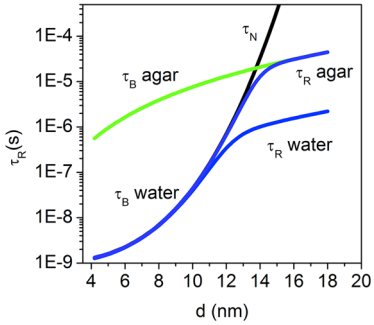

Figure 10. Relaxation times for MNPs dispersed in agar or water. The relaxation times τ_B, τ_N, and τ_R have been calculated with eqs 1, 2, and 3. We have considered a mean effective anisotropy $K_{eff} = 3 \times 10^4$ J/m^3.

due to the size distribution and to the close values of the Brown and Neel relaxation times (Table 2), both relaxation mechanisms are probably present in the larger mean MNP sizes. As can be seen from size distribution (Figure 1), sizes range from 8 to 16 nm when the mean particle size is 12.6 nm. For MNPs suspended in agar, the Brownian relaxation time of the largest particles is increased about 20 times (see eq 2), slowing down the particle rotation and inhibiting them from heat production, whereas the smallest ones still relax by a Neel mechanism, contributing thus to the heating. The presence of both Neel and Brown relaxation mechanisms in the 13 and 14 nm particles accounts for SAR decrease in the higher media viscosity. Therefore, it seems there is an optimal size (about 12 nm) at which heating production is a maximum regardless of media viscosity. Above this optimal size, the heating efficiency reduces with the increase of media viscosity, and below it decreases with particle volume. This is important for hyperthermia in cell culture media and tissues: large particle sizes with high SARs in aqueous colloid could not have the same heating efficiencies when the MNPs are introduced in a more viscous media, as is the case for cell culture media and tissues.

Table 3 shows the SAR values obtained for uncoated and APS-coated MNPs. The APS coating improves the colloidal properties and samples biocompatibility, but it could affect the heating efficiency since magnetic properties can be altered by the formation of the chemical bonds at the MNP surface or the formation of different aggregates. However, the samples measured before and after APS coating show similar heating efficiency under the same applied magnetic field. In addition, the SARs were obtained under experimental condition $H_0 f < 4 \times 10^9$ A/m^{-1} s^{-1} below the discomfort limit $D = 5 \times 10^9$ A/m^{-1} s^{-1}, a limit in the magnetic field conditions that is considered biomedically safe.[21] Therefore, the APS-coated γ-Fe_2O_3 MNPs is a very promising magnetic colloid for hyperthermia therapy in human cancer treatments.

4.3. Intrinsic Loss Power (ILP). The huge amount of data on the heating capacity of different MNPs under different conditions of MNPs concentration, field amplitude, and frequency makes it difficult to compare results and reach a consensus on the best material or the best measurements conditions. This is clearly limiting the transference of knowledge of this technology from the lab to the clinical application.

ILP values for commercial ferrofluids have been reported in the range 0.2−3.1 nHm^2/kg.[12] The calculated ILP value ILP = (SAR)/(fH_0^2) for the 13 nm MNPs is 1.78(1) nH m^2/kg for field amplitudes higher than 2.4 kA/m and at field frequency 522.3 kHz, a value which is high enough to make these MNPs applicable for hyperthermia treatments.

Despite the nonlineal frequency dependence of SAR observed in these MNPs, the ILP parameter seems to be a good candidate to characterize samples for hyperthermia treatments, especially for comparing heating efficiencies from different experimental conditions. The control of the heating capacity is essential to avoid overheating due to non-homogeneous MNPs biodistribution. Therefore, control on doses and fields are important.

5. CONCLUSIONS

These MNPs synthesized by coprecipitation method with acid treatment are an ideal material that allows the systematic study of the influence of size, concentration, carrier liquid, coating, and magnetic field amplitude and frequency on the particles heating efficiency. In addition, the APS coating that provides positive surface charge for further functionalization does not alter the heating capacity of the particle. It should be emphasized that the synthesis method used here for the MNPs preparation allows obtaining large amounts of particles in an easy, cheap, and reproducible procedure, and the SAR values have been obtained at frequency and magnetic field conditions that are considered biomedically safe.

The small size, low polydispersity, and high crystallinity degrees and the good magnetic behavior of the MNPs allow using LRT to understand the heating mechanisms. When the MNPs are dispersed in water, the SAR values are independent of NPs concentration in the range 6−300 mg/mL. Due to dilution procedure, the magnetic interactions remain almost unchanged inside the clusters, whereas the interaction between clusters seems to make a negligible contribution to MNPs heating capacity. The experimental SAR values as a function of field amplitude have a quadratic dependence, as expected from the model, for H_0 higher than 2.4 kA/m. The fitting of the SARs as function of field frequency allows obtaining the relaxation times τ_R which are about 10^{-7} s. These values are close to the calculated Brown relaxation times τ_B. It is possible to increase the Brownian relaxation times by increasing the media viscosity, allowing differentiating Neel or Brown relaxation mechanisms for the same NPs size. Larger MNPs (13 and 14 nm) dispersed in agar show a decrease in the SARs when compared with MNPs aqueous colloid of the same size, whereas the smaller particles (6, 8, and 11 nm) keep their heating efficiencies regardless of the media viscosity. These give hints to understand the relaxation mechanisms for each size:

dx.doi.org/10.1021/jp310771p | J. Phys. Chem. C 2012, 116, 25602−25610

due to size distribution and despite the low polydispersity degree, the larger mean MNPs size seems to relax by inversion of the magnetic moment in the monodomain (Neel relaxation) and by particle rotation (Brown relaxation) as both relaxation times are of the same order of magnitude. Therefore, there exists an optimal particle size at which heating efficiency is maximal and independent of media viscosity that in the case of these γ-Fe_2O_3 NPs is around 12 nm. This is important for in vitro and in vivo applications, where tissues have different viscosity.

Model behavior and good SAR values make these particles an ideal material for clinical applications and the standardization of hyperthermia equipment.

■ ASSOCIATED CONTENT

Supporting Information

Additional data about the HRTEM, XRD, FIRT, TG-DTA, and DLS experimental characterization of particles. This material is available free of charge via the Internet at http://pubs.acs.org.

■ AUTHOR INFORMATION

Corresponding Author

*E-mail: pm.presa@pdi.ucm.es.

Notes

The authors declare no competing financial interest.

■ ACKNOWLEDGMENTS

We thank F. Giacomone for the sample characterization of MNPs colloids in the Magnetherm equipment. This work was supported by grants from the Spanish Ministry of Science and Innovation (MAT2009-14741-C02-00, CSD2007-00010, MAT2011-23641), Madrid regional government CM (S009/MAT-1726), and Fundación Mutua Madrileña (Spain).

■ REFERENCES

(1) Hergt, R.; Andra, W.; d'Ambly, C. G.; Hilger, I.; Kaiser, W. A.; Richter, U.; Schmidt, H. G. *IEEE Trans. Magn.* **1998**, *34*, 3745.
(2) Hiergeist, R.; Andra, W.; Buske, N.; Hergt, R.; Hilger, I.; Richter, U.; Kaiser, W. *J. Magn. Magn. Mater.* **1999**, *201*, 420.
(3) Hergt, R.; Hiergeist, R.; Hilger, I.; Kaiser, W. A.; Lapatnikov, Y.; Margel, S.; Richter, U. *J. Magn. Magn. Mater.* **2004**, *270*, 345.
(4) Gupta, A. K.; Gupta, M. *Biomaterials* **2005**, *26*, 3995.
(5) Fortin, J. P.; Wilhelm, C.; Servais, J.; Menager, C.; Bacri, J. C.; Gazeau, F. *J. Am. Chem. Soc.* **2007**, *129*, 2628.
(6) Pankhurst, Q. A.; Thanh, N. K. T.; Jones, S. K.; Dobson, J. *J. Phys. D: Appl. Phys.* **2009**, 42.
(7) Villanueva, A.; de la Presa, P.; Alonso, J. M.; Rueda, T.; Martinez, A.; Crespo, P.; Morales, M. P.; Gonzalez-Fernandez, M. A.; Valdes, J.; Rivero, G. *J. Phys. Chem. C* **2010**, *114*, 1976.
(8) Mehdaoui, B.; Meffre, A.; Carrey, J.; Lachaize, S.; Lacroix, L. M.; Gougeon, M.; Chaudret, B.; Respaud, M. *Adv. Funct. Mater.* **2011**, *21*, 4573.
(9) Laurent, S.; Dutz, S.; Häfeli, U. O.; Mahmoudi, M. *Adv. Colloid Interface Sci.* **2011**, *166*, 8.
(10) Asin, L.; Ibarra, M. R.; Tres, A.; Goya, G. F. *Pharm. Res.* **2012**, *29*, 1319.
(11) Guardia, P.; Di Corato, R.; Lartigue, L.; Wilhelm, C.; Espinosa, A.; Garcia-Hernandez, M.; Gazeau, F.; Manna, L.; Pellegrino, T. *ACS Nano* **2012**, *6*, 3080.
(12) Kallumadil, M.; Tada, M.; Nakagawa, T.; Abe, M.; Southern, P.; Pankhurst, Q. A. *J. Magn. Magn. Mater.* **2009**, *321*, 1509.
(13) Glockl, G.; Hergt, R.; Zeisberger, M.; Dutz, S.; Nagel, S.; Weitschies, W. *J. Phys.: Condens. Matter* **2006**, *18*, S2935.
(14) Hergt, R.; Dutz, S.; Muller, R.; Zeisberger, M. *J. Phys.: Condens. Matter* **2006**, *18*, S2919.
(15) Costo, R.; Bello, V.; Robic, C.; Port, M.; Marco, J. F.; Morales, M. P.; Veintemillas-Verdaguer, S. *Langmuir* **2012**, *28*, 178.
(16) Abbasi, A. Z.; Gutierrez, L.; del Mercato, L. L.; Herranz, F.; Chubykalo-Fesenko, O.; Veintemillas-Verdaguer, S.; Parak, W. J.; Morales, M. P.; Gonzalez, J. M.; Hernando, A.; de la Presa, P. *J. Phys. Chem. C* **2011**, *115*, 6257.
(17) Gonzales-Weimuller, M.; Zeisberger, M.; Krishnan, K. M. *J. Magn. Magn. Mater.* **2009**, *321*, 1947.
(18) Levy, M.; Wilhelm, C.; Siaugue, J. M.; Horner, O.; Bacri, J. C.; Gazeau, F. *J. Phys.: Condens. Matter* **2008**, *20*, 204133.
(19) Johannsen, M.; Thiesen, B.; Wust, P.; Jordan, A. *Int. J. Hyperthermia* **2010**, *26*, 790.
(20) Wust, P.; Gneveckow, U.; Johannsen, M.; Bohmer, D.; Henkel, T.; Kahmann, F.; Sehouli, J.; Felix, R.; Ricke, J.; Jordan, A. *Int. J. Hyperthermia* **2006**, *22*, 673.
(21) Hergt, R.; Dutz, S. *J. Magn. Magn. Mater.* **2007**, *311*, 187.
(22) Massart, R. *IEEE Trans. Magn* **1981**, *17*, 1247.
(23) Morales, M. P.; Veintemillas-Verdaguer, S.; Montero, M. I.; Serna, C. J.; Roig, A.; Casas, L.; Martinez, B.; Sandiumenge, F. *Chem. Mater.* **1999**, *11*, 3058.
(24) van Ewijk, G. A.; Vroege, G. J.; Philipse, A. P. *J. Magn. Magn. Mater.* **1999**, *201*, 31.
(25) Mornet, S.; Portier, J.; Duguet, E. *J. Magn. Magn. Mater.* **2005**, *293*, 127.
(26) Gonzalez-Fernandez, M. A.; Torres, T. E.; Andres-Verges, M.; Costo, R.; de la Presa, P.; Serna, C. J.; Morales, M. R.; Marquina, C.; Ibarra, M. R.; Goya, G. F. *J. Solid State Chem.* **2009**, *182*, 2779.
(27) Natividad, E.; Castro, M.; Mediano, A. *J. Magn. Magn. Mater.* **2009**, *321*, 1497.
(28) Carrey, J.; Mehdaoui, B.; Respaud, M. *J. Appl. Phys.* **2011**, *109*, 083921.
(29) Fischer, B.; Huke, B.; Lucke, M.; Hempelmann, R. *J. Magn. Magn. Mater.* **2005**, *289*, 74.
(30) Parks, G. A. *Chem. Rev.* **1965**, *65*, 177.
(31) Garcell, L.; Morales, M. P.; Andres-Verges, M.; Tartaj, P.; Serna, C. J. *J. Colloid Interface Sci.* **1998**, *205*, 470.
(32) Gazeau, F.; Levy, M.; Wilhelm, C. *Nanomedicine* **2008**, *3*, 831.
(33) Hernando, A.; Vazquez, M.; Kulik, T.; Prados, C. *Phys. Rev. B* **1995**, *51*, 3581.
(34) Del Bianco, L.; Hernando, A.; Multigner, M.; Prados, C.; Sanchez-Lopez, J. C.; Fernandez, A.; Conde, C. F.; Conde, A. *J. Appl. Phys.* **1998**, *84*, 2189.
(35) de la Presa, P.; Rueda, T.; Hernando, A.; Ramallo-Lopez, J. M.; Giovanetti, L. J.; Requejo, F. G. *J. Appl. Phys.* **2008**, *103*, 103909.
(36) Goya, G. F.; Berquo, T. S.; Fonseca, F. C.; Morales, M. P. *J. Appl. Phys.* **2003**, *94*, 3520.
(37) Jeong, J. R.; Shin, S. C.; Lee, S. J.; Kim, J. D. *J. Magn. Magn. Mater.* **2005**, *286*, 5.
(38) Verges, M. A.; Costo, R.; Roca, A. G.; Marco, J. F.; Goya, G. F.; Serna, C. J.; Morales, M. P. *J. Phys. D: Appl. Phys.* **2008**, *41*, 134003.
(39) Bate, G. *Magnetic Oxides*; Wiley: London, U.K, 1975.
(40) Suzuki, H.; Sawai, Y.; Takada, M. *J. Jpn. Soc. Food Sci. Technol.—Nippon Shokuhin Kagaku Kogaku Kaishi* **1999**, *46*, 821.